

Proc. of the X Int. Conf. — Ion Implantation and other Applications of Ions and Electrons, Kazimierz Dolny 2014

Effect of N_2^+ Ion Implantation and Thermal Annealing on Near-Surface Layers of Implanted GaAs

M. KULIK^{a,b,*}, Z. SUROWIEC^a, W. RZODKIEWICZ^c, J. FILIKS^a AND A. DROZDZIEL^a^aInstitute of Physics, Maria Curie-Skłodowska University, pl. M. Curie-Skłodowskiej 1, 20-031 Lublin, Poland^bFrank Laboratory of Neutron Physics, Joint Institute for Nuclear Research, Joliot-Curie str. 6, Dubna, 141980, Moscow reg., Russia^cInstitute of Electron Technology, al. Lotników 32/46, 02-668 Warszawa, Poland

The surface of semi-insulating GaAs (100) was irradiated with a fluence of $6 \times 10^{17} \text{ cm}^{-2}$ of the N_2^+ ion beam; then, the samples were thermally annealed at temperatures of 500, 700, and 900 °C for 2 h in an argon gas flow. The surface roughness of implanted samples was investigated with the help of atomic force microscopy. Numerous hillocks, which caused a significant increase in surface roughness, were observed. The spectroscopic ellipsometry method was used for determination of pseudo-dielectric functions of the near-surface layers in the investigated samples and the thickness of native oxides covering the irradiated surface. It was observed that the shapes of disorder spectra of the dielectric functions of near-surface layers of implanted GaAs partly returned to their original state after the thermal annealing.

DOI: [10.12693/APhysPolA.128.918](https://doi.org/10.12693/APhysPolA.128.918)

PACS: 78.66.Fd, 78.68.+m, 79.20.Rf

1. Introduction

The ion implantation technique is a well-known method for the preparation of regions with different electrical conductivity and insulating areas in semiconductors [1, 2]. This method of doping materials has also been used to synthesis of InN by irradiated nitrogen ions to InP [3]. The structural and optical properties of GaAsN nanostructures, formed in the implanted epitaxial layer of GaAs are presented in [4]. In the cited papers, the process of ion irradiation was run at temperature of 300 °C and the nominal dose was $5 \times 10^{17} \text{ cm}^{-2}$. After irradiation, the samples were heat-treated by rapid thermal annealing (RTA) [4]. With the use of photoluminescence and the Raman spectroscopy as well as transmission electron microscopy (TEM) and grazing incidence X-ray diffraction (GIXRD), GaN and InN were found in the implanted layers, respectively. The results of the study on the formation and blistering of GaAsN nanostructure layers induced by N^+ implantation into crystalline samples of GaAs were reported [5].

In this paper, the investigations of surface quality and the dielectric functions of near-surface layers of semi-insulating GaAs implanted with N_2^+ ions and thermal annealing are described. Additionally, the thickness of native oxides and that of the regions enriched with oxygen atoms were determined with the use of spectroscopic ellipsometry (SE) as well as the Rutherford backscattering spectroscopy and nuclear reaction (RBS/NR), respectively.

2. Experimental

Monocrystals of semi-insulating GaAs (100) were implanted with N_2^+ ions at room temperature with the use of the UNIMAS implanter [6]. The energies of implantation ions were 120 keV and 160 keV, and the total fluence was $6 \times 10^{17} \text{ cm}^{-2}$. Then, the irradiated samples were covered with protective layers of Si_3N_4 and thermally annealed. These layers have been removed chemically after the process of annealing.

Their thickness was about 100 nm, and the annealing temperatures were 500, 700, and 900 °C. The annealing time was 2 h. The process of the isobaric thermal treatment was carried out in a flow of argon gas.

A Nanosurf EasyScan Atomic Force Microscopy (AFM) system was used to investigate the GaAs-implanted surface in order to obtain information about the surface roughness and evaluate the possible modifications of the topography after the implantation and annealing process. The AFM images (100 nm scans) were acquired by scanning the sample in air under ambient laboratory conditions (25 °C). The measurements were performed in a non-contact mode.

The AFM microphotographs were prepared using the VSXM program [7]. The roughness of the surface was assessed by measuring a roughness parameter, i.e. R_{rms} (root mean square roughness). R_{rms} is defined as the root mean square average of the height (h) deviations taken from the mean data plane. It is expressed as

$$R_{\text{rms}} = \sqrt{\frac{1}{N} \sum_{i=1}^N (h_i - \bar{h})^2}. \quad (1)$$

Here, h_i is the current height value, \bar{h} — the height of the mean data plane, and N is the number of points.

*corresponding author; e-mail:

mkulik@hektor.umcs.lublin.pl

The SE measurements of the investigated samples were carried out with the use of rotating analyser ellipsometry (RAE VASE). The ellipsometric spectra $\Psi(E)$ and $\Delta(E)$ were collected in the region of phonon energy from 1.2 eV to 5.0 eV at incidence angles of 65°, 70°, 75°, and 80°.

On the basis of the SE measurements, the spectra of average dielectric functions $\langle \varepsilon(E) \rangle$ of the near-surface layers of the analysed samples were calculated. In the first step, they were described with the two-phase model [8] (two homogeneous isotropic environments: ambient and studied material). This model with two media is very often used in the ellipsometric study of implanted semiconductors for example [9]. The following equations describe $\langle \varepsilon(E) \rangle$ [10]:

$$\langle \varepsilon(E) \rangle = n_0^2 \tan^2(\phi_{\text{in}}) \left[1 - \frac{4\rho}{(1+\rho)^2} \sin^2(\phi_{\text{in}}) \right], \quad (2)$$

where n_0 is the refraction coefficient of the environment, ϕ_{in} is the incidence angle. The value ρ is equal to

$$\rho = \tan \Psi e^{i\Delta}. \quad (3)$$

The spectra $\text{Re}\langle \varepsilon(E) \rangle$ and $\text{Im}\langle \varepsilon(E) \rangle$ were calculated by the point by point method [11] using the VASE32 code.

In the next step of the SE investigations, the thickness of the native oxide layers was determined. These layers were formed in the interactions between the atoms of the near-surface layers and the atoms of oxygen from air and oxides covering the analysed surface. In these calculations, the samples were approximated with the three-phase model (ambient, the layer of native oxide, and the substrate). This approach was used in the investigations of implanted semiconductors based on the ellipsometric method [12]. In the first approximation, it was assumed that the dielectric function of the oxide layers for the all analysed samples were the same like as for crystalline GaAs. These values are consistent with other investigations [13].

The near-surface layers of semiconductors: virgin GaAs and those subjected to the ion implantation and the thermal annealing were investigated by RBS/NR [14]. These measurements were carried out in JINR, Dubna using a Van de Graaff EG5 electrostatic generator.

Using the nuclear methods, the thickness of the layers enriched in oxygen atoms was determined. In these investigations, the resonance nuclear reaction $O^{16}(\alpha, \alpha)O^{16}$ was used [15]. The energy beam was in the range from 3.035 MeV to 3.060 MeV. The scattering spectra of α particles in the nucleons of the atoms in the analysed samples were collected at the scattering angle $\theta = 170^\circ$, and the angle between the direction of the incidence beam and the normal to the analysed surface was 15° . The detector resolution was 15 keV.

3. Results and discussions

Atomic force microscopy analysis illustrated the changes in surface topography generated on the GaAs

surface after the ion implantation. Figure 1 shows comparisons between the surface before (a) and after (b) the implantation process, where an increase in the surface roughness was observed after the ion implantation. Multiple measurements were taken in different surface regions, showing a R_{rms} of 1.2 nm for the unimplanted surface and 2.2 nm for the N-implanted region. Besides the increase in the R_{rms} , relatively deep pinholes appeared in the implanted surfaces. Those pinholes might have been a consequence of ion bombardment, as they could not be found on the untreated surface of GaAs.

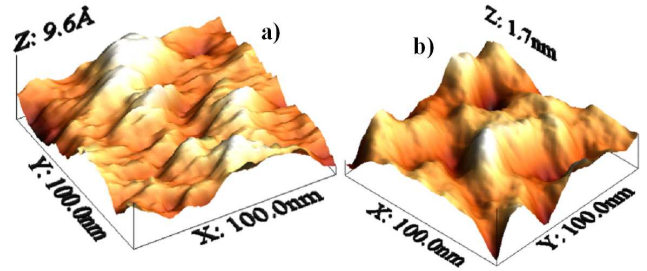


Fig. 1. AFM 3D images of 500 nm scans GaAs surface (a) before and (b) after implantation.

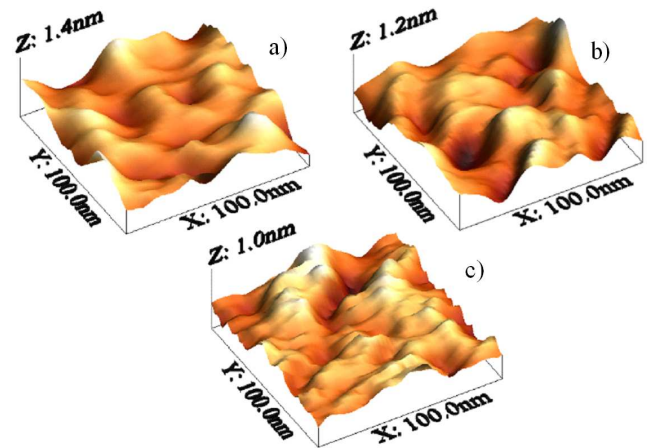


Fig. 2. AFM 3D images of 500 nm scans GaAs surface annealed at: (a) 500 °C, (b) 700 °C and (c) 900 °C.

The changes taking place on the surface of GaAs covered with a layer of Si_3N_4 and annealed at the temperature of 500, 700, and 900 °C are shown in Fig. 2. With the increase of the annealing temperature, the pinholes related to the implantation process became more flat. The R_{rms} parameter systematically decreased from the value 1.9 nm at the lowest annealing temperature to 1.4 nm at 900 °C.

The results of SE measurements for the virgin material are presented in Fig. 3. Two local maxima near the energy 3 eV can be observed in Fig. 3a and b. These bands are referred to the critical points (CP) E_1 and $E_1 + \Delta$ in the energy structure of crystalline GaAs [16]. The presence of these peaks confirms a good crystallographic structure for the initial samples used in

these investigations. It also suggests that the quality of the analysed surface is good and the results are in good agreement with Fig. 1a. It was noticed that the shapes of the ellipsometric curves in Fig. 3 (open and black rhombuses and black triangles) change in the energy range from 1.5 eV to 3.2 eV. The curves change their shape in comparison with the others, measured at smaller angles of incidence. This effect occurs with an increase in the incidence angle ϕ_{in} close to the principal angle [8]. This indicates that the SE measurement method in these conditions is characterized by high sensitivity. The surface of GaAs samples: crystalline, irradiated with nitrogen ions, and thermally annealed were measured with the SE method in the same conditions.

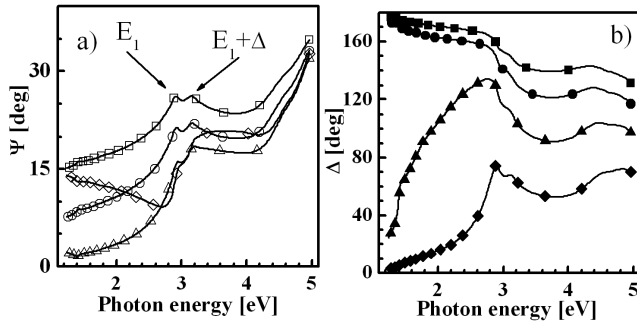


Fig. 3. Ellipsometric spectra measured for unimplanted GaAs: Ψ (a) and Δ (b). The open and full squares, circles, triangles and rhombuses correspond to values obtained at the incidence angles: 65° , 70° , 75° and 80° , respectively. The solid lines are the best-fit calculated curves.

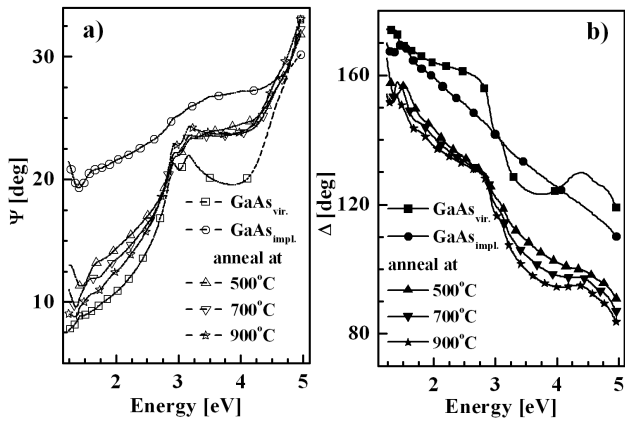


Fig. 4. Spectra: $\Psi(E)$ (dash lines and open symbols) and $\Delta(E)$ (solid lines and black symbols) measured at the incidence angle 70° for the all investigated samples.

Figure 4 presents typical ellipsometric measurements of $\Psi(E)$ and $\Delta(E)$ at the incidence angle 70° for the implanted and thermally annealed samples. These results are presented as a function of photon energy. It is shown in Fig. 4a and b that the bands near 3 eV related to the CPs, which are observed in the spectra measured for GaAs before the implantation, disappeared after ion beam irradiation of the surface of the crystalline material.

This effect is associated with damage of the crystalline structure of the near-surface layer of the sample. It is also observed that the values of $\Psi(E)$ increase and form a wide band from 2.9 eV to 4 eV after the ion implantation. In Fig. 4b, the values of $\Delta(E)$ (black disks) decrease with the increase in energy. This result confirms the formation of amorphous areas in the near-surface layer of GaAs.

The results of the measured spectra $\Psi(E)$ and $\Delta(E)$ in the regions from 1.2 eV to 1.9 eV and from 2.4 eV to 3.3 eV are shown in Fig. 5. The parts of these spectra are shown in Fig. 5a and b with bands at about 1.5 eV. This is observed for all curves except for the one measured for virgin materials. This effect can be explained by formation of a disordered layer. These layers have different optical constants than the substrate, thus the effects of light interference are visible. Figure 5c and d present the spectra near the energy bands E_1 and $E_1 + \Delta$ for crystalline GaAs. It can be noticed that the shape of the bands rebuilds with the increase of the annealing temperature, but the intensity of these bands is higher than that for virgin GaAs. During the thermal annealing process, the crystalline structure is probably partly rebuilt, the bubbles are formed in near-surface layers and gallium atoms diffuse into the surface. The same effect of diffusion of implanted elements to the irradiated surface was observed in [17].

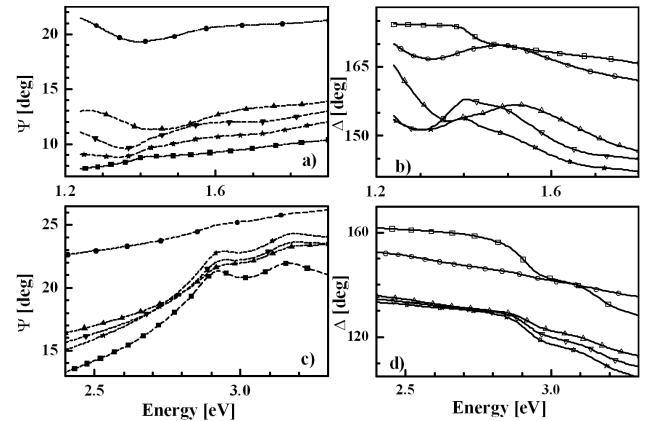


Fig. 5. The parts of spectra $\Psi(E)$ and $\Delta(E)$ GaAs before and after implantation and thermal annealing. Dash-point black and solid-point open lines represent the measurements values of Ψ and Δ angles, respectively. There are: squares — virgin GaAs, circles — implanted GaAs, and after thermal annealing at 500°C — \blacktriangle and open, at 700°C — \blacktriangledown and open, and at 900°C — black and open stars.

The spectra RBS/NR are shown in Fig. 6 with a band at *ca.* 1.1 MeV referred to the α particles scattered on the nucleons of oxygen. The intensity of the collected spectra decreases in the region from 2.1 MeV to 2.4 MeV. This effect is connected with the change in atomic density of gallium and arsenic atoms in implanted layers. On the basis of these measurements, the thickness of the layer enriched with oxygen atoms, the so-called native oxide

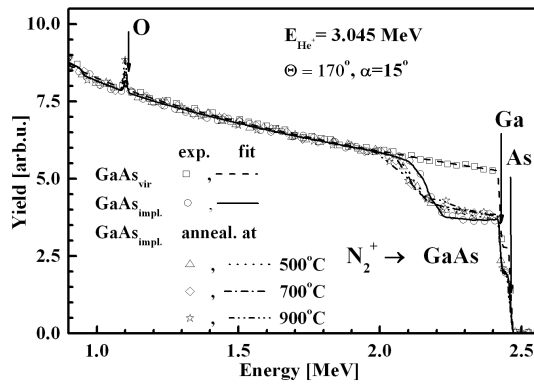


Fig. 6. RBS/NR spectra collected from the α particles scattered on the nucleons of atoms in the near surface layers of crystalline GaAs, and implanted and annealed GaAs.

TABLE

Thickness of the native oxide layers.

Name of the sample	Thickness of the native oxide layers [nm]		Surface atomic concentration RBS/NR [10^{14} at./ cm^2]		
	RBS/NR	Ellipsometry	Oxygen	Gallium	Arsenic
GaAs _{virgin}	2.5	2.1	5.7	52.1	52.1
GaAs _{impl}	6.0	5.1	21.1	78.8	48.7
annealing temperature [°C]	500	7.0	32.1	68.3	40.0
	700	8.0	42.9	87.2	41.9
	900	10.0	10.5	358.0	117.0

layer, was determined. In the calculations, it was assumed that the tested layers are homogeneous and they have the same atomic density as the crystalline GaAs. The atomic surface concentrations of oxygen, gallium, and arsenic in the near-surface layers were determined from the RBS/NR spectra. These values are shown in the Table. The SIMNRA code was used in the calculation and fitting of the experimental data [18, 19]. It is evident that the thickness of the native oxide layer increases after the ion implantation and simultaneously with the increase of the annealing temperature. The effects can be explained by the changes in the chemical composition of the near-surface layers. It was found that on the surface of the sample annealed at the temperature of 900 °C, the concentration of oxygen increased drastically compared to the values specified for the other samples. This effect can be explained by the changing chemical composition of this layer. It was observed that the concentration values of arsenic and gallium atoms decreased. The concentrations of the As and Ga atoms in this layer suggest the presence of mainly As_2O_5 and Ga_2O_3 oxides.

The results shown in Fig. 7 were calculated on the basis of SE measurements. In the calculations, Eqs. (2) and (3) were used. The spectrum of the imaginary part of the dielectric function has two local bands. One of them has two maxima referring to the positions of E_1 and $E_1 + \Delta$ and it is near 3.0 eV. The wider band is observed in the region 4.9 eV and is related to the E_1 transition. These structures are connected with the bands

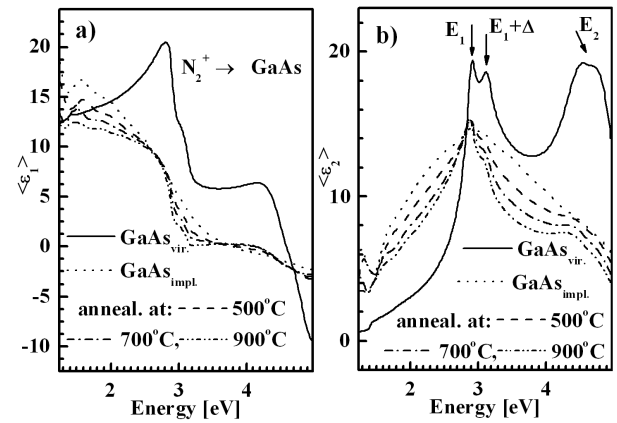


Fig. 7. The spectrum of average dielectric function are (a) real part, (b) imaginary part, determined for the examined GaAs lines: virgin — black, implanted — red, annealed at: green — 500 °C, blue — 700 °C and violet — 900 °C.

of crystalline GaAs and provide information that the near-surface layer of GaAs has a good crystalline quality. As noted in Fig. 4a and b, the shapes of the curves change after the implantation compared with the calculated spectra for the virgin material. A wide band with the maximum near 3.0 eV is presented in Fig. 4b. This is the effect of formation of amorphous GaAs in the near-surface layer after the ion implantation.

In the next step of the ellipsometric investigations, the thickness of the native oxides layer covering the analysed surface was determined. Here, the samples were described by means of the three-phase model. It consists of homogeneous isotropic media (an ambient and the substrate) with a plane layer of native oxides between them. The dielectric functions spectra determined in the first step and the thickness of the layers enriched with oxygen were the starting parameters for the determination of the optical properties on the near-surface layers. It was found that the thicknesses of the native oxides were in good agreement with the values obtained by nuclear methods; see the Table.

The results of calculations of the effective dielectric functions (see Eqs. (2), (3)) are presented in Fig. 7a and b. The change in spectral shape and values of the effective dielectric function following thermal annealing are observed. The first effect can be related to a partial reconstruction of the crystallographic structure of implanted samples. The process is manifested in the emergence of the E_1 and $E_1 + \Delta$ bands (see Fig. 7b). The change of the effective dielectric function values can be attributed to a change of the atomic composition of the subsurface atomic layers (see the Table).

4. Conclusions

The presented results indicate that due to the thermal annealing of nitrogen ion implanted samples, dielectric function changes occur in the near-surface layers of GaAs

and the spectra shapes partially return to their original state. The surface concentrations of oxygen in the layers of the native oxides increase with the temperature of annealing. The results of the RBS/NR investigations suggest that this effect may be related to the change in the chemical composition of implanted GaAs layers enriched with oxygen and formation of surface roughness. The AFM investigations have shown the pinholes of a 1.5 nm depth. This effect is observed in GaAs after implantation with nitrogen ions and annealing at a temperature of 900 °C.

References

- [1] S.J. Pearton, *Int. J. Mod. Phys. B* **7**, 4687 (1993).
- [2] A. White, K.T. Short, R.C. Dynes, R. Hull, S.M. Vandenberg, *Nucl. Instrum. Methods Phys. Res. B* **39**, 253 (1989).
- [3] K. Santhakumar, R. Kesavamoorthy, K.G.M. Nair, P. Jayavel, D. Kanjilal, V. Sankara Sastry, V. Ravichandran, *Nucl. Instrum. Methods Phys. Res. B* **212**, 521 (2003).
- [4] X. Weng, S.J. Clarke, W. Ye, S. Kumar, R.S. Goldman, A. Daniel, R. Clarke, J. Holt, J. Sipowska, A. Francis, V. Rotberg, *J. Appl. Phys.* **92**, 4012 (2002).
- [5] X. Weng, W. Ye, R.S. Goldman, J.C. Mabon, *J. Vac. Sci. Technol. B* **22**, 989 (2004).
- [6] M. Turek, S. Prucnal, A. Drozdziel, K. Pysznik, *Rev. Sci. Instrum.* **80**, 043304 (2009).
- [7] I. Horcas, R. Fernandez, J.M. Gomez-Rodriguez, J. Colchero, J. Gomez-Herrero, A.M. Baro, *Rev. Sci. Instrum.* **78**, 013705 (2007).
- [8] R.M.A. Azzam, N.M. Bashara, *Ellipsometry and Polarized Light*, North Holland, Amsterdam 1977.
- [9] R. Prabakaran, G. Raghavan, S. Tripura Sundari, R. Kesavamoorthy, *Solid State Commun.* **133**, 801 (2005).
- [10] H. Fujiwara, *Spectroscopic Ellipsometry Principles and Applications*, Wiley, West Sussex, England 2007.
- [11] T. Holden, P. Ram, F.H. Pollak, J.L. Freeouf, B.X. Yang, M.C. Tamargo, *Phys. Rev. B* **56**, 4037 (1997).
- [12] M. Fried, T. Lohner, W.A.M. Aarnink, L.J. Hanekamp, A. van Silfhout, *J. Appl. Phys.* **71**, 2835 (1992).
- [13] S. Zollner, *Appl. Phys. Lett.* **63**, 2523 (1993).
- [14] Wei-Kan Chu, J.W. Mayer, M.A. Nicolet, *Backscattering Spectrometry*, Academic Press, New York 1978.
- [15] J.R. Cameron, *Phys. Rev.* **90**, 893 (1953).
- [16] D.E. Aspnes, A.A. Studna, *Phys. Rev. B* **27**, 985 (1983).
- [17] M. Kulik, A.P. Kobzev, D. Jaworska, J. Zuk, J. Filiks, *Vacuum* **81**, 1124 (2007).
- [18] M. Mayer, *SIMNRA Home Page*, <http://home.rzg.mpg.de/~mam/>.
- [19] M. Mayer, *SIMNRA User's Guide*, Report IPP 9/113, Max-Planck-Institut für Plasmaphysik, Garching, Germany 1997.